NANO LETTERS

pubs.acs.org/NanoLett

Letter

A Tantalum Disulfide Charge-Density-Wave Stochastic Artificial Neuron for Emulating Neural Statistical Properties

Hefei Liu, Tong Wu, Xiaodong Yan, Jiangbin Wu, Nan Wang, Zhonghao Du, Hao Yang, Buyun Chen, Zhihan Zhang, Fanxin Liu, Wei Wu, Jing Guo, and Han Wang*

Cite This: *Nano Lett.* 2021, 21, 3465−3472

Read Online

ACCESS | Metrics & More | Article Recommendations | Supporting Information

ABSTRACT: Artificial neuronal devices that functionally resemble biological neurons are important toward realizing advanced brain emulation and for building bioinspired electronic systems. In this Communication, the stochastic behaviors of a neuronal oscillator based on the charge-density-wave (CDW) phase transition of a 1T-TaS_2 thin film are reported, and the capability of this neuronal oscillator to generate spike trains with statistical features closely matching those of biological neurons is demonstrated. The stochastic behaviors of the neuronal device result from the melt-quench-induced reconfiguration of CDW domains during each oscillation cycle. Owing to the stochasticity, numerous key features of the Hodgkin-Huxley description of neurons can be realized in this compact two-terminal neuronal oscillator. A statistical analysis of the spike train generated by the artificial neuron indicates that it resembles the neurons in the superior olivary complex of a mammalian nervous system, in terms of its interspike interval distribution, the time-correlation of spiking behavior, and its response to acoustic stimuli.

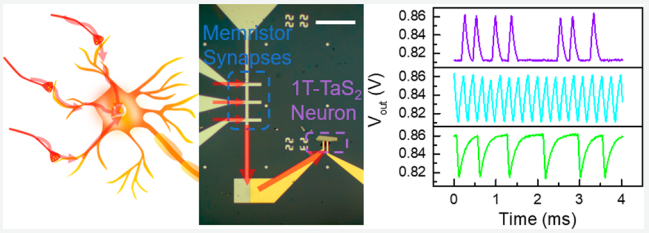

KEYWORDS: *charge-density-wave, stochastic artificial neurons, brain emulation, 1T-tantalum disulfide (1T-TaS_2)*

The stochastic nature plays a key role in enabling functions of biological neural networks including visual, auditory, and cognitive systems.[1−3] However, the research on the stochastic firing characteristic of artificial neurons remains very limited. Most previous research on artificial neurons has focused on developing circuits involving tens of transistors[4] or on building neuronal devices based on insulator−metal transition (IMT) materials,[5−8] volatile memristors,[9−11] magnetic tunnel junctions,[12,13] and chalcogenide-based phase-change materials,[14] to realize basic neuronal features such as emulating the action potential generation,[5,8,9] noise response,[15−17] and realizing the integrate-and-fire function for computing applications,[10,11,18] typically overlooking the stochasticity of neurons. Although there are a few reports of the stochastic artificial neurons based on IMT materials or spintronic devices,[8,14,19,20] the research on neuronal stochasticity is confined in the spike probability under different control conditions[19,20] or the response to input with stochastic noise.[8,14] Study on more detailed stochastic properties, such as the underlying form of probabilistic distribution followed by the interspike interval, the time correlation of spiking behavior, and the statistical resemblance to their biological counterpart, has been largely missing. In this work, we propose a stochastic neuronal oscillator utilizing the electrically induced charge-density-wave (CDW) phase transition of a 1T-TaS_2 thin film.[21−23] An oscillator device based on 1T-TaS_2 has been reported before.[21] However, the stochastic properties of the CDW device have never been studied. Here, we report the stochastic behaviors in the firing activity of the CDW neuronal oscillator. We discovered that tunable statistical characteristics can be achieved by applying different bias voltages to the device. Its close resemblance to the neuronal spiking in the superior olivary complex (SOC) of mammals is also revealed for the first time.

1T-TaS_2 is a layered crystalline material exhibiting typical CDW properties. At a high temperature there is a simple metallic phase. At T_{c0} = 543 K, it forms an incommensurate (IC) phase. When cooled below T_{c1} = 350 K, the IC structure forms a nearly commensurate (NC) state, where the hexagonal array of CDW domains are separated by domain walls. Below T_{c2} = 183 K, a fully commensurate (C) phase forms.[24] Figure 1a illustrates the atomic structure of the four phases. The C phase behaves as a Mott insulator, but IC is metallic. The NC phase is an intermediate phase. The atomic structure of CDW domains and domain walls resemble C and IC, respectively.[25−27] At room temperature, 1T-TaS_2 thin films are normally in the NC phase, but they would undergo a phase

Received: January 9, 2021
Revised: April 2, 2021
Published: April 9, 2021

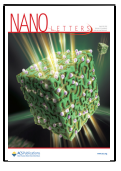

https://doi.org/10.1021/acs.nanolett.1c00108
Nano Lett. 2021, 21, 3465−3472

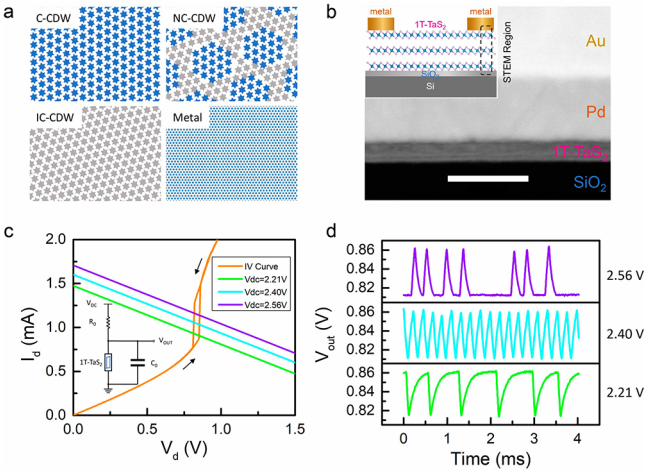

Figure 1. Structure and electrical characterization of a 1T-TaS_2 oscillator. (a) Schematic illustration of the atomic structure of the four phases of 1T-TaS_2. Blue and gray stars represent CDW superlattice in C and IC phases, respectively. The blue dots in the metal phase schematic represent individual Ta atoms. (b) Schematic structure and cross-sectional STEM image of the 1T-TaS_2 oscillator at the metal contact region. The scale bar is 20 nm. The thickness of this 1T-TaS_2 sample is ~6 nm. (c) $I-V$ characteristic of the 1T-TaS_2 film, the oscillator circuitry, and the load lines under different bias conditions. The oscillation occurs if V_{dc} ranges from 2.21 V (green line) to 2.56 V (violet line). (d) The corresponding oscillation waveforms at different V_{dc} in (c). For V_{dc} = 2.21 V (green) and V_{dc} = 2.56 V (violet), the oscillation peaks are separated by random time intervals; for V_{dc} = 2.40 V (cyan line), the oscillation occurs continuously.

transition to IC in the presence of an external electric field exceeding 20 kV cm^{-1}, accompanied by the resistance decreasing to approximately half of its initial value,[21,22,28] which makes a room-temperature oscillator possible.

Figure 1b shows the schematic structure of the 1T-TaS_2 neuronal oscillator and the cross-sectional scanning transmission electron microscopy (STEM) image at the metal contact region. The material composition of each layer is confirmed by the electron energy loss spectroscopy (EELS), as shown in Figure S1 (Supporting Information). In the current−voltage ($I-V$) characteristics of the 1T-TaS_2 device (Figure 1c, orange curve), an abrupt current increase at the threshold voltage (V_{th}) was observed due to the phase transition from NC to IC.[21,26,27] To induce the oscillation, a series resistor and a parallel capacitor are connected to the device to form a Pearson-Anson circuit, and then a DC bias (V_{dc}) is applied. The voltage across the 1T-TaS_2 thin film (V_{out}) is observed by an oscilloscope. If the load line of the resistor in the circuit crosses the hysteresis window like the straight lines do in Figure 1c, the 1T-TaS_2 thin film can convert back and forth between the NC and IC states, leading to the oscillation of V_{out}.[21] The waveform of oscillation can be tuned by the applied V_{dc} (Figure 1d). When V_{dc} is around the lower limit of oscillation (Figure 1c green line, 2.21 V), the 1T-TaS_2 thin film tends to stay mostly in the NC phase, only occasionally switching to the IC phase, and switches back to NC immediately (Figure 1d, green waveform). Since the time interval between the consecutive pulses is random, this operation domain can be considered as the stochastic oscillation regime. The oscillation behavior is similar when the voltage is close to the upper limit (Figure 1c violet line,

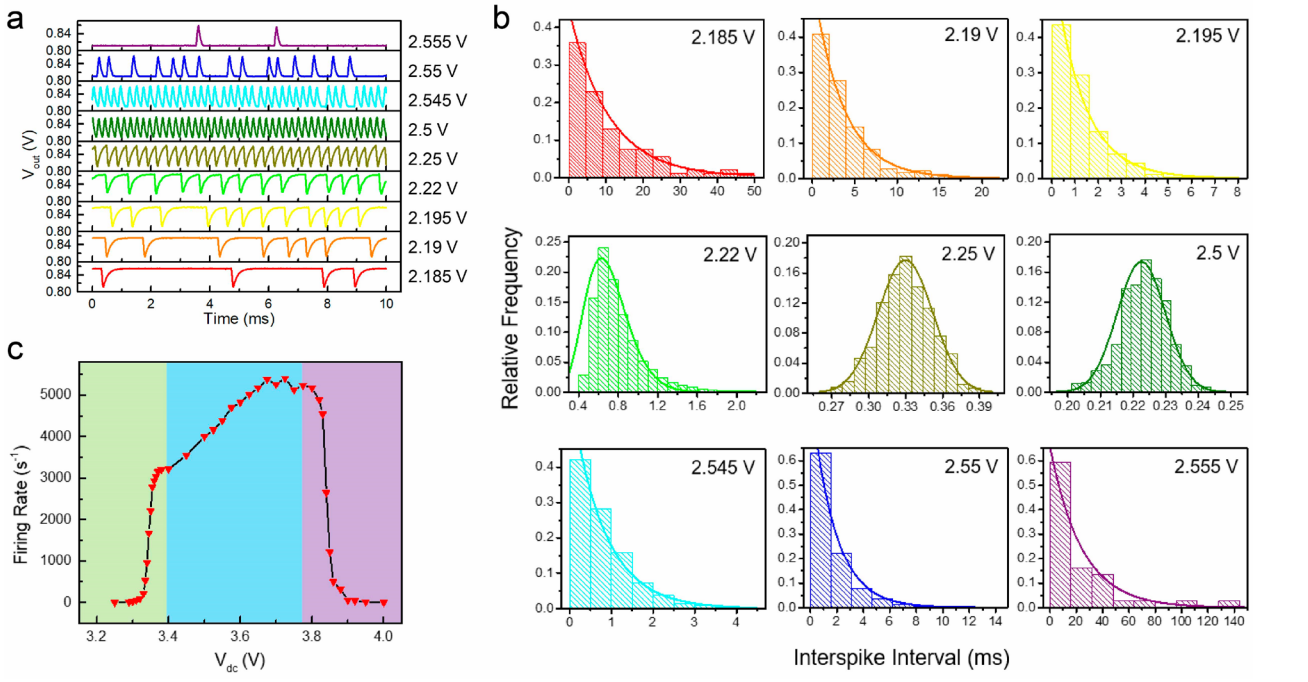

Figure 2. Statistical analysis of the spike trains generated by the artificial neuron. (a) A typical series of waveforms excited by increasing V_{dc}. The series resistor is 1.5 kΩ. (b) The statistical distribution of the interspike intervals corresponding to the different bias conditions as indicated in (a) and the fitted distribution curves. For the stochastic oscillation regime, the interspike interval generally follows an exponential distribution with tunable rate parameter λ = 0.0937 ms^{-1} (2.185 V), 0.283 ms^{-1} (2.19 V), 0.781 ms^{-1} (2.195 V), 1.248 ms^{-1} (2.545 V), 0.575 ms^{-1} (2.55 V), 0.0414 ms^{-1} (2.555 V). For the regular oscillation regime, the interval follows a Gaussian distribution with tunable mean μ and standard deviation σ, μ = 0.330 ms and σ = 0.0221 ms (2.25 V), μ = 0.223 ms and σ = 0.0074 ms (2.25 V). A transitional Gamma distribution with parameters α = 10 and β = 0.07 is also observed (2.22 V). (c) Firing rate vs V_{dc} relation of the neuronal oscillator with a 3 kΩ series resistor.

https://doi.org/10.1021/acs.nanolett.1c00108
Nano Lett. 2021, 21, 3465−3472

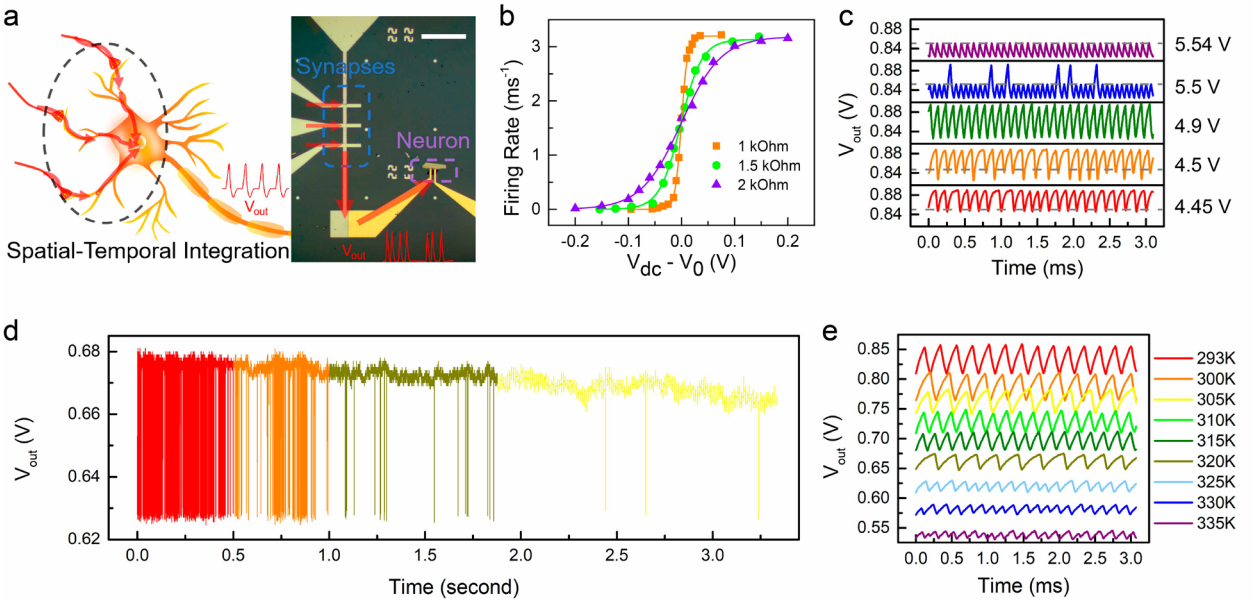

Figure 3. Demonstration of key features of biological neurons using the neuronal oscillator. (a) Optical micrograph of a 3-synapse-1-neuron network that consists of three memristors connected in parallel to the 1T-TaS_2 device, as well as the comparison to its biological analogue. The scale bar is 100 μm. (b) The firing rate vs V_{dc} relation with different series resistances to mimic the firing rate vs membrane potential of a biological neuron. (c) Subthreshold oscillation of the neuronal device. Voltage levels of the metastable state are denoted by gray dash lines. (d) Frequency adaption of the memristor-oscillator network. (e) Temperature dependence of the neuronal oscillator. As the temperature approaches T_{c1} of the phase transition (350 K), the output waveform shifts downward, and the oscillation amplitude shrinks, similar to the behavior of typical biological neurons.[43,44]

2.56 V), but in this case the 1T-TaS_2 tends to remain in the IC phase (Figure 1d, violet waveform). When V_{dc} is between the two stochastic oscillation regimes (Figure 1c cyan line, 2.40 V), neither NC nor IC is relatively stable, resulting in a continuous oscillation waveform where every pulse is closely followed by another (Figure 1d, cyan line). We consider this operation domain as the regular oscillation regime.

To investigate the stochastic properties of the 1T-TaS_2 device and its ability to emulate the stochasticity in biological neural spiking, a statistical analysis of the spike trains generated by the artificial neuron was conducted. Following the similar approach as the statistical treatment of an actual nervous cell, we focused on the analysis of the interspike time intervals.[29−32] Figure 2a shows a typical series of spike trains generated by the 1T-TaS_2 artificial neuron under different bias conditions. The oscillation waveforms of only 10 ms duration of the measured data are displayed so that the interspike intervals can be clearly distinguished. Figure 2b shows the histograms of the interspike intervals and the fitted distribution curves corresponding to each waveform in Figure 2a. Generally, when the device operates in the stochastic oscillation regime, the interspike interval follows exponential distributions with tunable rate parameter λ ranging from 0.041 to 1.248 ms^{-1}. When the device operates in the regular oscillation regime (dark yellow and olive lines), randomness still exists due to the varying oscillation amplitude, which results from the resistance variation of the 1T-TaS_2 thin film during each oscillation cycle (Figure S2, Supporting Information). In this case, the interspike intervals follow a Gaussian distribution whose mean and standard deviation (std) both decrease as V_{dc} increases. In addition, an intermediate distribution (green line) is also found when V_{dc} is very close to the regular oscillation regime, which can be fitted well using a Gamma distribution. The two parameters of the Gamma distribution (α, β) can change from (2, 1.5) to (12, 0.06) as V_{dc} increases, leading to a gradual transition from exponential to Gaussian (Figure S3, Supporting Information). The spike trains with interspike intervals following exponential, Gamma, and Gaussian distributions were also observed in biological neurons of a mammalian auditory nerve.[33,34]

Figure 2c plots the firing rate as a function of V_{dc}. For the regular oscillation (blue region), the firing rate is determined by the RC (R = resistor; C = capacitor) delay of the circuit. The upward trend of firing rate in this regime is due to the larger current enhancing the charge/discharge rate of the capacitor. At both sides (green and purple regions) of this plot, the device is in the stochastic oscillation regime, where the dependence of the firing rate on the bias voltage is very sensitive. An abrupt rise of the firing rate occurs as V_{dc} comes closer to the regular oscillation regime by less than 0.1 V.

To investigate the origin of the stochastic oscillation, we measured the *IV* curve of a 1T-TaS_2 sample for over 200 switching cycles, with a 1 min cooling down between each two measurements as a precaution to exclude potential heat accumulation; results are shown in Figure S5 (Supporting Information). The V_{th} of the phase transition has a cycle-to-cycle variation within the range from 0.823 to 0.840 V, which results from the microscopic stochasticity in the CDW phase transition process. When the device operates in the stochastic oscillation regime, the oscillator operation is very sensitive to the varying V_{th}. A slight variation in V_{th} can lead to the change between firing and nonfiring. In other words, the microscopic stochasticity in the CDW transition process is magnified in the oscillator operation. As a result, the stochastic oscillation regime exhibits a significantly enhanced randomness and stochastic features compared to the regular oscillation regime.

A numerical model is developed to describe how the random distribution of the threshold voltage leads to the stochastic

https://doi.org/10.1021/acs.nanolett.1c00108
Nano Lett. 2021, 21, 3465−3472

oscillation. A sigmoidal dependence of the firing rate as a function of the threshold voltage is extracted from experiment. The firing rate increases from 0 to over 3000 s^{-1} when the threshold voltage changes by only ~0.02 V. With this relation as the input, we simulated the spike trains generated under different bias conditions in the lower stochastic oscillation regime using a Monte Carlo method. The spike waveforms and the exponential distributions of the interspike interval obtained from the simulation agree well with the experimental results, as shown in Figure 2a,b and Figure S6 (Supporting Information). This serves as a validation that the stochastic behaviors of the neuronal oscillator originate from the V_{th} variation of the 1T-TaS_2 device. We attribute the distribution of V_{th} to the microscopic random rearrangement of CDW domains during each phase transition cycle, which results from the melting-and-quench process induced by the joule heat when current passes through the 1T-TaS_2 thin film.[35−39] The existence of CDW domains has been confirmed by scanning tunneling microscopy, and the domain reconfiguration has been captured by ultrafast dark-field electron microscopy in a recently published paper.[25−27,40−42] The CDW domain reconfiguration can change the resistance of the thin film and therefore the V_{th} of phase transition.

The firing rate−voltage relation shown in Figure 2c demonstrates that information can be coded and transmitted by the spiking frequency in this oscillator device, which implies the potential of the device as a neuron emulator. To study how the oscillator device performs as an artificial neuron, we integrated three parallel memristors as artificial synapses to the oscillator. Figure S7 (Supporting Information) shows the characteristics of the memristor, and Figure 3a shows the optical image of the system. Using the 3-synapse-1-neuron network, we demonstrated numerous critical features of a biological neuron.[43,44] Since the three memristors share the same bottom electrode, the spatial-temporal integration can be directly realized based on Ohm's law and Kirchhoff's current law (Figure S8, Supporting Information).

Figure 3b plots the firing rate as a function of V_{dc} when the devices with different series resistors operate in the lower stochastic oscillation regime. For clarity, the curves are shifted with respect to their respective bias voltage V_0 at which the firing probability is half. The dependence of the firing rate on bias voltage can be described by a logistic function, which closely matches the firing rate versus membrane voltage relation of typical biological neurons.[29−32] Furthermore, the slope of the curve can be readily tuned by changing the value of the series resistance, which provides the capability to emulate a wide range of probabilistic models of artificial neuron, including the present model, linear model, or sigmoidal model depending on specific application needs.[45]

Subthreshold oscillation, another key feature of biological neurons, can be realized in a neuronal oscillator with a relatively thick 1T-TaS_2 film (~20 nm). Besides the two stable states (NC at ~0.89 V and IC at ~0.825 V), a metastable intermediate state at ~0.85 V is observed in the $I-V$ characteristic (Figure S10, Supporting Information), which can be ascribed to the nonuniform temperature distribution in the sample according to a previous study.[46] When operating in the stochastic oscillation regime, the 1T-TaS_2 sample sometimes can be "stuck" in this intermediate state and then directly return to the initial state, and it only occasionally experiences a complete phase transition (Figure 3c, V_{dc} = 4.5 or 5.5 V). Such a waveform can be regarded as a train of neural spikes separated by subthreshold oscillations. When V_{dc} further decreases to 4.45 V (or increases to 5.54 V), a pure subthreshold oscillation can be realized.

We also demonstrated the neuronal frequency adaption in the memristor-oscillator network, by exploiting the filament reshaping of memristor when electric current passes through it. Figure 3d shows the waveform evolution in a larger time scale (~3.5 s). As time proceeds, the resistance of the memristor increases, as shown in Figure S7c (Supporting Information). Hence the voltage across the 1T-TaS_2 thin film reduces gradually. The oscillation evolves from regular (red) to stochastic (orange). It then experiences a further decrease in the frequency (dark yellow) and finally almost terminates (yellow).

In addition, we measured oscillation waveforms from room temperature to 335 K to show the temperature dependence of the artificial neuron. Both the average voltage level and the amplitude of the oscillation reduce as the environmental temperature increases, as shown in Figure 3e, which arises due to the shift and shrink of the hysteresis window at a higher temperature (Figure S11, Supporting Information). Such a temperature dependence of the neuronal spiking closely mimics the temperature-dependent behavior of biological neurons as described by the Hodgkin-Huxley model.[43,44]

To further demonstrate the capability of the 1T-TaS_2 stochastic neuronal device for emulating the statistical features of biological neurons, we replicated the behaviors of neurons in the SOC of mammals (dogs and cats) using the 1T-TaS_2 device operating in the lower stochastic regime, with reference to the previous physiological research on these biological neurons.[34,47] Other than the similarities demonstrated in the distribution of interspike intervals, the mean versus std relation is also plotted in Figure 4a. It is clear that all points locate around a straight line, which validates the exponential distribution of interspike intervals. The spike trains generated by both the artificial neuron and the neurons of the HDR-I unit of cats' SOC both show this pattern and imply that the interspike interval is independent of history (see Figure S12 in the Supporting Information for comparison).[29,30] To further confirm this, we established a generalized linear model (GLM) in which the dependence of the current spike interval (interval index difference m = 0) on the past 10 intervals (m = 1,2,...,10) are considered (Figure 4b). The analysis of the spike trains of the two stochastic oscillation regimes (orange for the lower, violet for the upper) and one regular oscillation regime (green) shows that the Kernel parameter (which reflects the degree of correlation) of all the historical events are much smaller than that of the current event itself by 1−2 orders of magnitude, as shown in Figure 4b. It means that the correlation between the current spike and historical spikes is very weak, if not completely independent. This inference is also supported by the autocorrelation analysis as shown in the inset of Figure 4b, points symmetrically distributed on both sides of the x-axis, with a maximum deviation of ~0.4. Such results also resemble the autocorrelation of the spike trains generated by the neurons in cats' HDR-I unit (see Figure S12 in the Supporting Information for comparison).[34] When the firing rate is high (very close to a regular oscillation regime), a polynomial relation between the mean and std of the intervals, together with a weak autocorrelation, is observed. The behavior of the device in this regime is closer to the neurons of HDR-II or LDR units in cats' SOC (see Figure S13 in the Supporting Information for a comparison).[34]

https://doi.org/10.1021/acs.nanolett.1c00108
Nano Lett. 2021, 21, 3465−3472

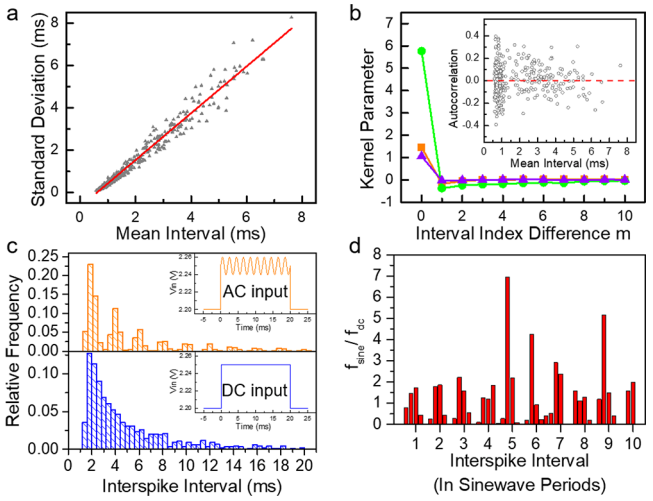

Figure 4. Emulation of the statistical properties of the neurons in the SOC of mammalian nervous systems. (a) Mean vs standard deviation relation of the artificial neural spiking. Each point is based on data derived from 80 consecutive intervals. (b) Time correlation analysis of the artificial neural spiking. The kernel parameter vs the interval index difference m relation derived from the GLM model shows that for both the regular (green) and stochastic oscillation regimes (orange for lower, violet for upper) the interspike interval depends mainly on the current state (m = 0) rather than the history of the spike train (m = 1,2,...,10). (inset) The autocorrelation coefficient vs mean interval relation of the spike train in the stochastic regime. (c) The artificial neuron's response to DC excitation (blue) and 500 Hz sinusoidal excitation (orange) in terms of interspike interval distribution. (insets) The applied input voltage waveforms. (d) The response of the neuronal device to sinusoidal excitation f_{sine} normalized to the baseline response to DC input f_{dc} for each column in (c).

The SOC is the first major site of convergence of auditory information from ears and can transmit frequency information to brains, which may also be used to fulfill tasks like Fourier transform in electronic devices. Therefore, we made a comparison between the response of the 1T-TaS_2 neuronal oscillator to a 500 Hz sinusoidal excitation input and that of biological neurons in the mammalian auditory system. Figure 4c shows the distribution of interspike intervals when the neuronal oscillator is excited by a sinewave input (f_{sine}) and by a DC input (f_{dc}). As discussed above, the interspike intervals should follow an exponential distribution. However, with a sinewave input, the neuronal response shows an extra sinusoidal modulation in the interval histogram besides the overall trend of exponential decay. To highlight the difference, the ratio of f_{sine} to f_{dc} in each time division of Figure 4c was calculated and shown in Figure 4d. For clarity of display, in Figure 4d the period of the input sinewave (2 ms) is used as the unit of time. Compared with the response of the neuronal device to the DC input, the interspike intervals in response to the sinusoidal excitation are more likely to distribute around the integer multiples of the input sinewave period. Such a behavior normalized to the baseline response to DC input, that is, f_{sine}/f_{dc}, closely matches the response of the biological neurons in unit 67−28−5 of dogs' medial superior olive to monotone acoustic stimuli (see Figure S15 in the Supporting Information for a comparison).[47] In biological auditory neurons, the congregation of the interspike intervals around integer multiples of the excitation input period plays a critical role in the human and animal's ability to transmit the frequency information on acoustic stimuli.[47] Hence, the statistical similarity in the spike trains not only reveals the resemblance of the artificial neuron to its biological counterpart but also is a requirement for neuronal devices to enable more sophisticated neuronal functions.

In summary, the 1T-TaS_2 stochastic neuronal oscillator demonstrated here is capable of generating spiking trains with statistical characteristics closely matching those of biological neurons. Tunable stochastic spiking characteristics following exponential, Gaussian, and Gamma distributions were realized by this artificial neuron. The stochasticity is due to the varying threshold voltage of phase transition, which originates from the microscopic random reconfiguration of CDW domains in the 1T-TaS_2 thin film during each oscillation cycle. By integrating the neuronal device with memristors or a fixed resistor to form an oscillating circuitry, we captured many key features of biological neurons as described by the Hodgkin-Huxley model, such as frequency coding, frequency adaption, temperature dependence, and subthreshold oscillation. Furthermore, when a sinusoidal input excites the neuronal oscillator, a change in the distribution pattern of interspike intervals can emulate the response of mammals' auditory neurons to acoustic stimuli. Therefore, the stochastic neuronal oscillator offers not only an approach for better neuron emulation but also a new perspective toward designing the neuron component of spiking neural networks, exploiting more sophisticated neuronal behaviors such as the stimulus-adaptive statistical properties to encode and transmit information.

METHODS

Device Fabrication and Electrical Characterization. 1T-TaS_2 crystals were provided by HQ Graphene. Nanometer-thick samples were isolated from the bulk crystal using mechanical exfoliation and transferred onto a p-doped silicon wafer with 90 nm thermally grown silicon dioxide. Metal contacts were fabricated using electron beam lithography patterning followed by the deposition of palladium (15 nm) and gold (50 nm) metals using electron beam evaporation. The thickness of the sample was determined by atomic force microscopy (Bruker Dimension Icon) and transmission electron microscopy. The memristor devices were integrated with the 1T-TaS_2 device on the same wafer substrate. The bottom electrodes consist of 2 nm titanium and 20 nm platinum, and the top electrodes consist of 8 nm tantalum and 30 nm platinum. The switching layer is 5 nm Al_2O_3 deposited at 80 °C using atomic layer deposition. All $I-V$ characteristics were measured in the Lakeshore cryogenic probe station TTPX with a semiconductor analyzer (Keysight B1500A). The oscillation waveform is collected by an oscilloscope (Keysight DSO-X 3024T). The sinewave signal is generated by an intrinsic function generator in the oscilloscope.

STEM and EELS Measurement. The high-resolution STEM image was obtained using an FEI Titan Themis G2 with four detectors and spherical aberration. Before the measurement, the sample was coated by chromium and carbon layers on top sequentially, for protection, and then thinned by the focused ion beam (FIB, FEI Helios 450S) with an acceleration voltage of 30 kV. The acceleration voltage was increased to 200 kV during the imaging to improve the image quality. The EELS signals were collected by the Gatan 977 integrated within the STEM system.

Monte Carlo Simulation. The sigmoidal dependence of the firing rate on the threshold voltage is propositional to the cumulative distribution function of the threshold voltage $V_{th}^{(i)}$}

https://doi.org/10.1021/acs.nanolett.1c00108
Nano Lett. 2021, 21, 3465−3472

derived from an experimental result. The firing rate is simulated as

$$\lambda(V_0^{(i)}) = \lambda_0\left(1 - \frac{1}{1 + \alpha\ \exp(V_0^{(i)}/\gamma)}\right) \quad (1)$$

where λ_0 is the firing rate when the oscillation is about to be continuous, $V_0^{(i)} = V_b - V_{th}^{(i)}$, and V_b is the applied bias voltage across the 1T-TaS_2 thin film, $\alpha = 3.5$ is a fitting coefficient, and $\gamma = 0.002$ eV is a broadening of the frequency transition. The $\{V_0^{(i)}\}$ are drawn from the Gaussian distribution $N(V_b - V_{th,mean}, \sigma(\{V_{th}^{(i)}\}))$, which is extracted from the experimental data. The interspike interval $t^{(i)} - t^{(i-1)}$ is simulated as the expected first arrival time of a Poisson point process with rate $\lambda(V_0^{(i)})$.

Generalized Linear Model. The GLM allows the outcome of dependent variables Y generated from a particular distribution in the exponential dispersion models. In the GLM model, the mean value μ depends on the independent variables X as

$$\mu = E(Y|X) = g^{-1}(X\beta) \quad (2)$$

where $E(Y|X)$ is the expected value of Y, $X\beta$ is the linear predictor, and g is the link function. To analyze the experimental data, the effect of the historical and current interspike intervals (X) on current interspike interval (Y) is considered in the linear part of the model that uses the kernel parameters (β) to quantify the temporal correlation between the neural spikes. Comparison between the experimental and theoretical data shows that the log link function $X\beta = \ln(\mu)$, which corresponds to the Poisson distribution. The extracted kernel parameter $\beta(m)$, as shown in Figure 4b, describes the effect the spiking activity at the time bin $(t - m)$ on the spiking activity at the time bin t, which quantifies the temporal correlation property of the experimental spiking data.

■ ASSOCIATED CONTENT

Supporting Information

The Supporting Information is available free of charge at https://pubs.acs.org/doi/10.1021/acs.nanolett.1c00108.

EELS data, cycle-to-cycle variation of device resistance and threshold voltage, complete oscillation waveforms under different bias voltages, simulated neural spike trains and interspike interval distributions, electrical characteristics of memristors used in the main article, IV curves of 1T-TaS_2 at different temperatures, and comparison of statistical properties between the neuronal oscillator and biological neurons (PDF)

■ AUTHOR INFORMATION

Corresponding Author

Han Wang − *Ming Hsieh Department of Electrical and Computer Engineering and Mork Family Department of Chemical Engineering and Materials Science, University of Southern California, Los Angeles 90089, California, United States;* orcid.org/0000-0001-5121-3362; Email: han.wang.4@usc.edu

Authors

Hefei Liu − *Ming Hsieh Department of Electrical and Computer Engineering, University of Southern California, Los Angeles 90089, California, United States;* orcid.org/0000-0001-6533-7112

Tong Wu − *Department of Electrical and Computer Engineering, University of Florida, Gainesville 32611, Florida, United States;* orcid.org/0000-0001-6018-0283

Xiaodong Yan − *Ming Hsieh Department of Electrical and Computer Engineering, University of Southern California, Los Angeles 90089, California, United States;* orcid.org/0000-0002-7737-6984

Jiangbin Wu − *Ming Hsieh Department of Electrical and Computer Engineering, University of Southern California, Los Angeles 90089, California, United States*

Nan Wang − *Mork Family Department of Chemical Engineering and Materials Science, University of Southern California, Los Angeles 90089, California, United States*

Zhonghao Du − *Ming Hsieh Department of Electrical and Computer Engineering, University of Southern California, Los Angeles 90089, California, United States;* orcid.org/0000-0001-5199-850X

Hao Yang − *Ming Hsieh Department of Electrical and Computer Engineering, University of Southern California, Los Angeles 90089, California, United States;* orcid.org/0000-0002-0992-9161

Buyun Chen − *Ming Hsieh Department of Electrical and Computer Engineering, University of Southern California, Los Angeles 90089, California, United States;* orcid.org/0000-0001-8326-6688

Zhihan Zhang − *School of Electrical and Computer Engineering, Georgia Institute of Technology, Atlanta 30332, Georgia, United States*

Fanxin Liu − *Collaborative Innovation Center for Information Technology in Biological and Medical Physics, and College of Science, Zhejiang University of Technology, Hangzhou 310023, China;* orcid.org/0000-0003-0445-3886

Wei Wu − *Ming Hsieh Department of Electrical and Computer Engineering, University of Southern California, Los Angeles 90089, California, United States;* orcid.org/0000-0001-6404-0317

Jing Guo − *Department of Electrical and Computer Engineering, University of Florida, Gainesville 32611, Florida, United States;* orcid.org/0000-0003-4009-3056

Complete contact information is available at: https://pubs.acs.org/10.1021/acs.nanolett.1c00108

Author Contributions

H.L. contributed to the development of the idea for the experiment, performed device fabrication, conducted the measurements and the data analysis, and wrote the manuscript. T.W. conducted the numerical simulation and contributed to manuscript writing. X.Y., J.W., N.W., Z.D., and Z.Z. contributed to the measurements of the 1T-TaS_2 oscillator. H.Y., B.C., and W.W. fabricated and characterized the memristors. F.L. performed the TEM characterization. J.G. designed the numerical simulation and contributed to the manuscript writing. H.W. had the idea for the experiment, contributed to the manuscript writing, and supervised the whole project. All the authors discussed the results and commented on the manuscript.

Notes

The authors declare the following competing financial interest(s): Han Wang currently also serves as the research principal investigator at TSMC Corporate Research.

https://doi.org/10.1021/acs.nanolett.1c00108
Nano Lett. 2021, 21, 3465−3472

■ ACKNOWLEDGMENTS

This work is supported in part by the Army Research Office Young Investigator Program (Grant No. W911NF-18-1-0268) and the National Science Foundation (Grant No. ECCS-1653870). T.W. and J.G. were supported by National Science Foundation (Grant Nos. 1904580 and 1809770). H.Y., B.C., and W.W. were supported by Air Force Research Laboratory (Grant No. FA8750-19-1-0503).

■ REFERENCES

(1) Oram, M.; Wiener, M.; Lestienne, R.; Richmond, B. Stochastic nature of precisely timed spike patterns in visual system neuronal responses. *J. Neurophysiol.* **1999**, *81*, 3021−3033.
(2) Siebert, W. M. Some implications of the stochastic behavior of primary auditory neurons. *Kybernetik* **1965**, *2*, 206−215.
(3) Rolls, E. T.; Deco, G. *The noisy brain: stochastic dynamics as a principle of brain function;* Oxford University Press: Oxford, UK, 2010; Vol. *34*.
(4) Al-Shedivat, M.; Naous, R.; Cauwenberghs, G.; Salama, K. N. Memristors empower spiking neurons with stochasticity. *IEEE Journal on Emerging and Selected Topics in Circuits and Systems* **2015**, *5*, 242−253.
(5) Pickett, M. D.; Medeiros-Ribeiro, G.; Williams, R. S. A scalable neuristor built with Mott memristors. *Nat. Mater.* **2013**, *12*, 114.
(6) Chen, P.-Y.; Seo, J.-S.; Cao, Y.; Yu, S. In *2016 IEEE/ACM International Conference on Computer-Aided Design (ICCAD);* IEEE, 2016; pp 1−6.
(7) Moon, K.; et al. In *2015 IEEE International Electron Devices Meeting (IEDM),* 17.16. 11−17.16. 14; IEEE, 2015.
(8) Yi, W.; et al. Biological plausibility and stochasticity in scalable VO2 active memristor neurons. *Nat. Commun.* **2018**, *9*, 4661.
(9) Huang, H. M.; et al. Quasi-Hodgkin−Huxley Neurons with Leaky Integrate-and-Fire Functions Physically Realized with Memristive Devices. *Adv. Mater.* **2019**, *31*, 1803849.
(10) Wang, Z.; et al. Fully memristive neural networks for pattern classification with unsupervised learning. *Nature Electronics* **2018**, *1*, 137.
(11) Yoon, J. H.; et al. An artificial nociceptor based on a diffusive memristor. *Nat. Commun.* **2018**, *9*, 417.
(12) Romera, M.; et al. Vowel recognition with four coupled spin-torque nano-oscillators. *Nature* **2018**, *563*, 230−242.
(13) Torrejon, J.; et al. Neuromorphic computing with nanoscale spintronic oscillators. *Nature* **2017**, *547*, 428.
(14) Tuma, T.; Pantazi, A.; Le Gallo, M.; Sebastian, A.; Eleftheriou, E. Stochastic phase-change neurons. *Nat. Nanotechnol.* **2016**, *11*, 693.
(15) Lee, I. Y.; Liu, X.; Kosko, B.; Zhou, C. Nanosignal processing: Stochastic resonance in carbon nanotubes that detect subthreshold signals. *Nano Lett.* **2003**, *3*, 1683−1686.
(16) Kang, Q.; Huang, B.; Zhou, M. Dynamic behavior of artificial Hodgkin−Huxley neuron model subject to additive noise. *IEEE transactions on cybernetics* **2016**, *46*, 2083−2093.
(17) Chow, C. C.; Imhoff, T. T.; Collins, J. J. Enhancing aperiodic stochastic resonance through noise modulation. *Chaos* **1998**, *8*, 616−620.
(18) Gao, L.; Chen, P.-Y.; Yu, S. NbOx based oscillation neuron for neuromorphic computing. *Appl. Phys. Lett.* **2017**, *111*, 103503.
(19) Jerry, M.; Parihar, A.; Grisafe, B.; Raychowdhury, A.; Datta, S. In *2017 Symposium on VLSI Circuits;* IEEE, 2017; T186−T187.
(20) Cai, J.; et al. Voltage-controlled spintronic stochastic neuron based on a magnetic tunnel junction. *Phys. Rev. Appl.* **2019**, *11*, 034015.
(21) Liu, G.; et al. A charge-density-wave oscillator based on an integrated tantalum disulfide−boron nitride−graphene device operating at room temperature. *Nat. Nanotechnol.* **2016**, *11*, 845.
(22) Hollander, M. J.; et al. Electrically driven reversible insulator−metal phase transition in 1T-TaS2. *Nano Lett.* **2015**, *15*, 1861−1866.
(23) Grüner, G. The dynamics of charge-density waves. *Rev. Mod. Phys.* **1988**, *60*, 1129.
(24) Sipos, B.; et al. From Mott state to superconductivity in 1T-TaS2. *Nat. Mater.* **2008**, *7*, 960.
(25) Thomson, R.; Burk, B.; Zettl, A.; Clarke, J. Scanning tunneling microscopy of the charge-density-wave structure in 1T-TaS 2. *Phys. Rev. B: Condens. Matter Mater. Phys.* **1994**, *49*, 16899.
(26) Tsen, A. W.; et al. Structure and control of charge density waves in two-dimensional 1T-TaS2. *Proc. Natl. Acad. Sci. U. S. A.* **2015**, *112*, 15054−15059.
(27) Spijkerman, A.; de Boer, J. L.; Meetsma, A.; Wiegers, G. A.; van Smaalen, S. X-ray crystal-structure refinement of the nearly commensurate phase of 1*T*−TaS_2 in (3 + 2)-dimensional superspace. *Phys. Rev. B: Condens. Matter Mater. Phys.* **1997**, *56*, 13757.
(28) Yoshida, M.; Suzuki, R.; Zhang, Y.; Nakano, M.; Iwasa, Y. Memristive phase switching in two-dimensional 1T-TaS_2 crystals. *Science Advances* **2015**, *1*, No. e1500606.
(29) Perkel, D. H.; Gerstein, G. L.; Moore, G. P. Neuronal spike trains and stochastic point processes: I. The single spike train. *Biophys. J.* **1967**, *7*, 391−418.
(30) Perkel, D. H.; Gerstein, G. L.; Moore, G. P. Neuronal spike trains and stochastic point processes: II. Simultaneous spike trains. *Biophys. J.* **1967**, *7*, 419−440.
(31) Tuckwell, H. C.; Richter, W. Neuronal interspike time distributions and the estimation of neurophysiological and neuroanatomical parameters. *J. Theor. Biol.* **1978**, *71*, 167−183.
(32) Wilbur, W. J.; Rinzel, J. A theoretical basis for large coefficient of variation and bimodality in neuronal interspike interval distributions. *J. Theor. Biol.* **1983**, *105*, 345−368.
(33) Teich, M. C.; Khanna, S. M. Pulse-number distribution for the neural spike train in the cat's auditory nerve. *J. Acoust. Soc. Am.* **1985**, *77*, 1110−1128.
(34) Goldberg, J. M.; Adrian, H. O.; Smith, F. D. Response of neurons of the superior olivary complex of the cat to acoustic stimuli of long duration. *J. Neurophysiol.* **1964**, *27*, 706−749.
(35) Wu, X. L.; Lieber, C. M. Direct observation of growth and melting of the hexagonal-domain charge-density-wave phase in 1T-TaS 2 by scanning tunneling microscopy. *Phys. Rev. Lett.* **1990**, *64*, 1150.
(36) Ma, L.; et al. A metallic mosaic phase and the origin of Mott-insulating state in 1T-TaS 2. *Nat. Commun.* **2016**, *7*, 10956.
(37) Wu, X. L.; Lieber, C. M. Hexagonal domain-like charge density wave phase of TaS2 determined by scanning tunneling microscopy. *Science* **1989**, *243*, 1703−1705.
(38) Slough, C.; et al. Atomic force microscopy and scanning tunneling microscopy of charge-density waves in 1T-TaSe2 and 1T-TaS2. *Phys. Rev. B: Condens. Matter Mater. Phys.* **1990**, *42*, 9255.
(39) Burk, B.; Thomson, R.; Zettl, A.; Clarke, J. Charge-density-wave domains in 1T-TaS2 observed by satellite structure in scanning-tunneling-microscopy images. *Phys. Rev. Lett.* **1991**, *66*, 3040.
(40) Nakanishi, K.; Takatera, H.; Yamada, Y.; Shiba, H. The nearly commensurate phase and effect of harmonics on the successive phase transition in 1T-TaS2. *J. Phys. Soc. Jpn.* **1977**, *43*, 1509−1517.
(41) Nakanishi, K.; Shiba, H. Domain-like incommensurate charge-density-wave states and the first-order incommensurate-commensurate transitions in layered tantalum dichalcogenides. I. 1T-polytype. *J. Phys. Soc. Jpn.* **1977**, *43*, 1839−1847.
(42) Danz, T.; Domröse, T.; Ropers, C. Ultrafast nanoimaging of the order parameter in a structural phase transition. *Science* **2021**, *371*, 371−374.
(43) Kandel, E. R.; et al. *Principles of Neural Science;* McGraw-Hill: New York, 2000; Vol. *4*.
(44) Bear, M. F.; Connors, B. W.; Paradiso, M. A. *Neuroscience;* Lippincott Williams & Wilkins, 2007; Vol. *2*.
(45) Hopfield, J. J. Neural networks and physical systems with emergent collective computational abilities. *Proc. Natl. Acad. Sci. U. S. A.* **1982**, *79*, 2554−2558.
(46) Geremew, A. K.; et al. Bias-Voltage Driven Switching of the Charge-Density-Wave and Normal Metallic Phases in 1T-TaS2 Thin-Film Devices. *ACS Nano* **2019**, *13*, 7231−7240.

https://doi.org/10.1021/acs.nanolett.1c00108
Nano Lett. 2021, 21, 3465−3472

(47) Goldberg, J. M.; Brown, P. B. Response of binaural neurons of dog superior olivary complex to dichotic tonal stimuli: some physiological mechanisms of sound localization. *J. Neurophysiol.* **1969**, *32*, 613−636.

https://doi.org/10.1021/acs.nanolett.1c00108
Nano Lett. 2021, 21, 3465−3472